Biosensors and Bioelectronics: X 31 (2026) 100809

Contents lists available at ScienceDirect

Biosensors and Bioelectronics: X

journal homepage: www.journals.elsevier.com/biosensors-and-bioelectronics-x

Low-cost colourimetric biosensing using laser-patterned cellophane-based fluidic devices

Ahsan Ali [a,*], Panagiotis Galanis [b], Jonathan McQuillan [b], Kordo Saeed [c,d], Ahilanandan Dushianthan [c,e], Gopalan K. Sivaraman [f], Collin L. Sones [a]

[a] Optoelectronics Research Centre, University of Southampton, Southampton, SO17 1BJ, UK
[b] National Oceanography Centre, Southampton, SO14 3ZH, UK
[c] Clinical and Experimental Sciences, Faculty of Medicine, University Hospital Southampton NHS Foundation Trust, Southampton, SO16 6YD, UK
[d] Department of Infection, University Hospital Southampton NHS Foundation Trust, Southampton, SO16 6YD, UK
[e] General Intensive Care Unit, University Hospital Southampton NHS Foundation Trust, Southampton, SO16 6YD, UK
[f] Microbiology, Fermentation & Biotechnology Division, ICAR- Central Institute of Fisheries Technology, Cochin-29, Kerala, India

ARTICLE INFO

Keywords:
Cellophane
Laser direct-write
Photo-polymerisation
Colourimetric assay
Point-of-care diagnostics
Glucose
Nitrite

ABSTRACT

Cellophane is an attractive low-cost substrate for environmentally sustainable fluidic devices because it is biodegradable. Here, we report a laser direct-write (LDW) method, which relies on the principle of photo-polymerisation of a light-sensitive polymer for rapid fabrication of cellophane-based fluidic devices. In this method, a photo-polymer is first deposited on a cellophane substrate in a user-defined pattern and subsequently illuminated using a 405 nm laser to photo-polymerise the pre-deposited patterns and form hydrophobic polymer structures that form the walls of open wells and enclosed flow channels. By tuning the photo-polymer deposition speeds and deposition–photo-polymerisation cycles, polymerised structures with widths of 0.5–2 mm and heights of 0.1–2 mm were reproducibly fabricated on both uncoated and polymer-coated cellophane. Enclosed flow channels with coated cellophane as both layers supported pump-driven flow at 50–250 μL min^{-1}, while hybrid channels with an uncoated bottom layer and coated top layer enabled pump-free capillary transport. Quantitative colourimetric detection of glucose (GOx/HRP–o-dianisidine assay) and nitrite (Griess reaction) was implemented within open wells. The limit-of-detection and limit-of-quantification were 7.31/23.8 μg mL^{-1} and 6.57/21.9 μM across the ranges of 10–100 μg mL^{-1} and 5–200 μM for glucose and nitrite respectively. We also report the detection of glucose and nitrite in artificial urine samples within both open well and enclosed flow channels. This LDW-based fabrication approach provides a practical and flexible route for rapid prototyping of disposable cellophane-based fluidic devices for colourimetric sensing.

1. Introduction

The increasing demand for single use, low-cost and environmentally sustainable diagnostics for clinical, environmental, water and food quality testing has driven continued interest in microfluidics for point-of-need applications (Hu et al., 2014). Microfluidic devices offer distinct advantages including miniaturisation, portability, reduced reagent consumption and integration of multistep workflows with minimal operator handling, thereby enabling rapid assays with improved analytical performance (Hu et al., 2014; Solanki et al., 2020; Whitesides, 2006; Yager et al., 2006). Despite these merits, factors such as high fabrication cost, the requirement of specialised ancillary equipment, and the use of non-biodegradable materials have significantly hindered the widespread and large scale adoption of these devices for commercial use (Dincer et al., 2019; Gubala et al., 2012; Ongaro et al., 2022; Shigemori et al., 2023).

The COVID-19 pandemic has underscored the crucial need for rapid and affordable point-of-care diagnostics and highlighted the importance of developing technologies capable of addressing current and emerging diagnostic challenges (Budd et al., 2023). This has generated a renewed and increased interest in microfluidic-based technologies that can facilitate rapid, accurate, portable and cost-effective diagnostic solutions (Tarim et al., 2023). The pandemic has also reiterated a growing emphasis on the development of environmentally sustainable

* Corresponding author. Optoelectronics Research Centre, Building 46, University Road, Southampton SO17 1BJ, UK.
E-mail address: ahsan.ali@soton.ac.uk (A. Ali).

https://doi.org/10.1016/j.biosx.2026.100809
Received 16 April 2026; Received in revised form 9 June 2026; Accepted 17 June 2026
Available online 22 June 2026

alternatives whilst maintaining device performance (Zimmer et al., 2026).

Over the past two decades, paper-based microfluidic devices have demonstrated strong potential as inherently low-cost and environmentally sustainable alternatives for testing across a range of applications, predominantly point-of-care diagnostic testing within under-resourced settings (Hamedi et al., 2016; Martinez et al., 2010; Noviana et al., 2021; Shigemori et al., 2023). Within the ever-expanding field of microfluidics, there have been recent studies that have reported the use of cellophane as a substrate for fabrication of microfluidic devices (Hamedi et al., 2016; Shigemori et al., 2023). These reports suggest that cellophane can complement the advantages offered by paper, enabling the development of environmentally sustainable and low-cost sensing platforms.

Cellophane shares many key attributes inherent to paper such as low-cost (<1USD m^{-2}), abundant availability, biocompatibility and biodegradability (Hamedi et al., 2016; Zhang et al., 1996). In contrast to paper, cellophane possesses the additional advantageous attributes of optical transparency across the entire visible and UV spectrum, which is comparable to glass and most plastics, making it particularly suitable for applications involving optical detection of analytes (Yang et al., 2011). In addition, cellophane exhibits resistance to both organic and aqueous solvents such as methanol, ethanol and water, which are commonly used in biological assays (Hamedi et al., 2016; Makarov et al., 2022).

Its inherent hydrophilicity (Yamane et al., 2006) and permeability (Shigemori et al., 2023) to water are primarily advantageous for facilitating pump-free liquid transport and enabling the immobilisation of water-soluble reagents for colourimetric assays respectively. Collectively, these characteristics position cellophane not only as a complementary alternative to paper, but also a sustainable substitute for traditional microfluidic materials including cyclic olefin polymers, polydimethylsiloxane (PDMS), poly (methyl-methacrylate) (PMMA), glass and quartz (Hamedi et al., 2016).

The Whitesides' group was the first to showcase the benefits of using cellophane for making fluidic devices and it reported the use of specially designed embossing moulds, double-sided tape and lamination sheets in a multistep fabrication method (Hamedi et al., 2016). To address the challenges highlighted by the Whitesides' group, the Citterio group later presented a different fabrication method requiring multiple steps of printing, cutting and laminating cellophane sheets, but again, they highlight the challenges related to the complexity of their multistep approach (Shigemori et al., 2023). These only two previously reported methods for the fabrication of cellophane-based devices involve multiple steps which are time-consuming, expensive and complex to implement and therefore undesirable for large-scale and cost-effective mass manufacturing - in turn, negating the affordability advantage made available through the use of cellophane. To unlock the full potential of cellophane for affordable point-of-care diagnostics, however, there still exists a clear need for a simple, scalable and economically viable fabrication method.

Here, we report a laser direct-write (LDW) fabrication method for rapid prototyping and cost-effective mass-manufacturing of cellophane-based fluidic devices. This method has previously been reported for creating paper-based microfluidic devices for applications including antibiotic resistance testing, and performance improvements such as 3D paper-based devices, filtration, sensitivity enhancement and multiplexing on a lateral flow test using laser-patterned flow channels (Galanis et al., 2022; He et al. 2016, 2018, 2020; Katis et al., 2018; Sones et al., 2014). This laser-based method requires a basic laboratory environment and a semi-skilled operator and involves first the deposition of a photo-polymer onto a cellophane substrate in a user-defined pattern, followed by illumination from a continuous wave laser source that traces the same pattern to create solid polymeric structures that define a range of fluidic geometries including straight and curved flow channels and circular wells. We also demonstrate the use of the flow channels in the transport of fluids under passive capillary-driven and pump-driven conditions and more importantly, implementation of quantitative colourimetric assays for the detection of nitrite and glucose within flow channels and open wells. Collectively, this work presents the viability of using a LDW technique for rapid fabrication of disposable fluidic devices on cellophane for applications including simple, visual colourimetric sensing.

2. Materials and methods

2.1. Materials and reagents

Uncoated cellophane (42NP, 42 μm thickness) and hydrophobic polymer-coated cellophane (45NK, 45 μm thickness) films were supplied by Futamura Chemical Co., Ltd. (Japan). The polymer used for the fabrication of the fluidic devices was an acrylate-based negative photo-polymer (DeSolite® 3471-3-14, with viscosity of 10000 mPa s at 25 °C) procured from DSM Desotech, Inc. (USA). All other reagents, including Brilliant Blue FCF, Allura Red, sodium nitrite, bromophenol blue, citric acid, trisodium citrate dihydrate, sulfanilamide, N-(1-Naphthyl) ethylenediamine dihydrochloride, glucose oxidase/peroxidase reagent, α-D-Glucose, o-dianisidine dihydrochloride, and isopropanol (IPA), were purchased from Sigma-Aldrich (UK). A PICO® Pμlse™ dispenser platform (Nordson EFD, UK) and a fibre-coupled 405 nm continuous wave (c.w.) diode laser (Cobolt MLD™, Cobolt AB Sweden) were used for the deposition and polymerisation.

2.2. Fluidic device fabrication using laser direct-write (LDW)

2.2.1. LDW system and parameter optimisation

Fluidic devices were fabricated on cellophane substrates using a custom LDW technique (Fig. 1A). The photo-polymer was first deposited in a user-defined pattern on a cellophane substrate using a non-contact jetting valve (Nordson EFD PICO Pμlse®). The jetting valve operated in a continuous dispensing mode and was maintained at a temperature of 70 °C and a pneumatic pressure of 2 psi. The deposition patterns were programmed using the Nordson EFD's proprietary Dispense Motion software. Following deposition, the photo-polymer pattern was cured using a 405 nm continuous wave laser. To scan over the previously deposited photo-polymer patterns with minimal adjustments, the robotic arm/gantry of the Nordson EFD PICO Pμlse® system was adapted to integrate the laser next to the jetting valve. The laser illumination initiates photo-polymerisation of the deposited polymer to create solid, hydrophobic structures that either define (the walls of the) open wells or the fluidic channels.

At 405 nm, the photoinitiator in the acrylate-based polymer absorbs the incident laser light to generate free radicals that initiate crosslinking that converts the deposited liquid polymer into a solid network (Sones et al., 2014). The laser fluence used in this study (~40 mJ cm^{-2}) was higher than the reported minimum fluence (~0.4 mJ cm^{-2}) required to cure DeSolite polymer, and no visible damage to the cellophane substrate was observed for these illumination conditions.

A parametric study was performed to identify the photo-polymer deposition and laser illumination parameters that produce continuous and well-defined structures. Deposition speeds (30–100 mm s^{-1}), laser illumination speeds (30–60 mm s^{-1}), and deposition-polymerisation cycles (1–20) were varied systematically while maintaining other system parameters constant. To ensure consistency, the distance between the jetting valve and the cellophane substrate was kept constant (7 mm). For each parameter, line structures were fabricated and subsequently assessed for continuity and feature dimension (wall width and height). The optimised parameters devised from this study were used for subsequent device fabrication.

2.2.2. Fabrication of open wells

As shown in Fig. 1A, devices with an array of circular open wells were patterned on both coated and uncoated cellophane to mimic one of

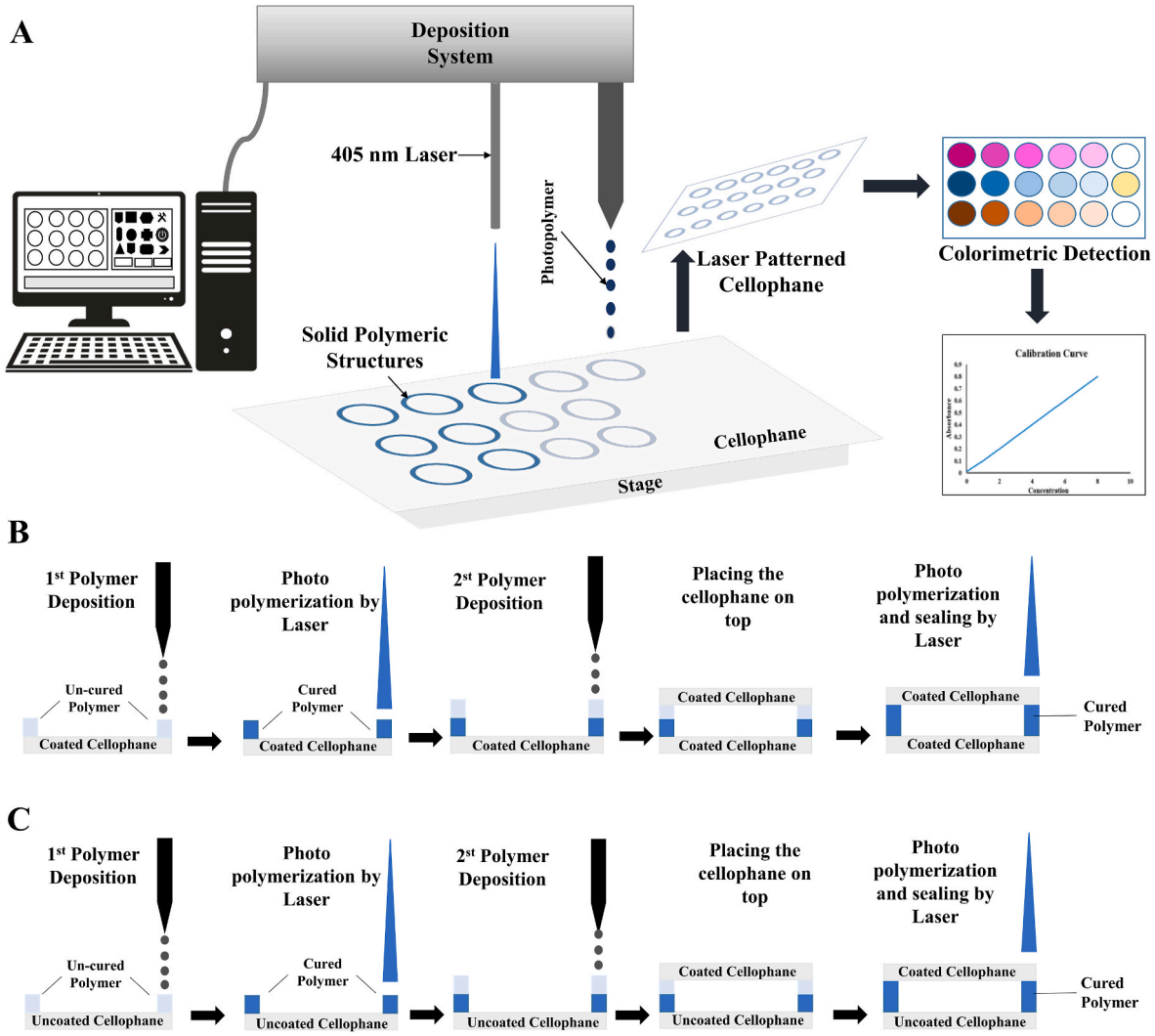

Fig. 1. Laser direct-write (LDW) fabrication of cellophane-based fluidic devices. Schematic of the LDW process used to fabricate (A) open wells on coated and uncoated cellophane, (B) Enclosed flow channels using coated cellophane as bottom and top layers: a cured base pattern is first formed on the bottom film, followed by deposition of a second identical polymeric pattern that is laser-cured after positioning of the top film to form sealed device and (C) Hybrid enclosed flow channel configuration fabricated using the same two-layer deposition and laser-curing approach but instead using an uncoated cellophane as the bottom layer and coated top sealing layer.

the most routinely used assay platforms, a 96-well plate. Each well had a diameter of 7.5 mm and a wall height of 0.5 mm. Polymer walls defining the wells were formed using a deposition speed of 50 mm s^{-1}, which was followed by laser illumination at 30 mm s^{-1} (incident fluence ~ 40 mJ cm^{-2}) with a 15 s delay between deposition and curing. A total of five deposition-polymerisation cycles were used to achieve well heights that ensure desired liquid containment.

2.2.3. Fabrication of enclosed flow channels

Enclosed flow channels (on both coated and uncoated cellophane) were fabricated using a multi-layer technique described in Fig. 1B and C. First, a photo-polymer pattern that defined the shape of a flow channel was deposited onto the bottom cellophane sheet and subsequently cured with the 405 nm laser. Next, a second, identical photo-polymer pattern was deposited directly on top of the first cured base pattern. Before this second photo-polymer pattern is cured, a second cellophane sheet was placed over the uncured polymer. The photo-polymer pattern was then illuminated through the top cellophane sheet to cure the second pattern and in turn bond the top and bottom cellophane sheets to produce sealed flow channels.

To ensure optimal bonding which eliminates any leakage, deposition speed of 50 mm s^{-1} and laser illumination speed of 30 mm s^{-1} were used. In addition, the following two different device configurations were explored and compared: (i) one using coated cellophane for both the top and bottom (Fig. 1B), and (ii) a hybrid configuration using an uncoated cellophane as bottom layer and a coated cellophane as the top layer (Fig. 1C).

2.3. Characterisation of open wells and enclosed flow channels

The topography of LDW patterned polymeric structures, which act as fluid containing barrier walls, was characterised prior to validating their properties to hold and guide fluids. Barrier line profiles (Fig. 2B and D) were measured using a stylus profilometer (Tencor P16). For each set of patterning parameters, three identical line structures were produced on three separate devices and mean ± SD of the height and width of patterned structures were calculated. The height and width of the walls were extracted from the profilometer traces to correlate the LDW processing conditions with the resulting feature dimensions. In addition, images of the laser-patterned line structures (Fig. 2A and C) formed on both uncoated and polymer-coated cellophane were acquired using an Epson V800 flatbed scanner (600 dpi). Optical microscopy was used to

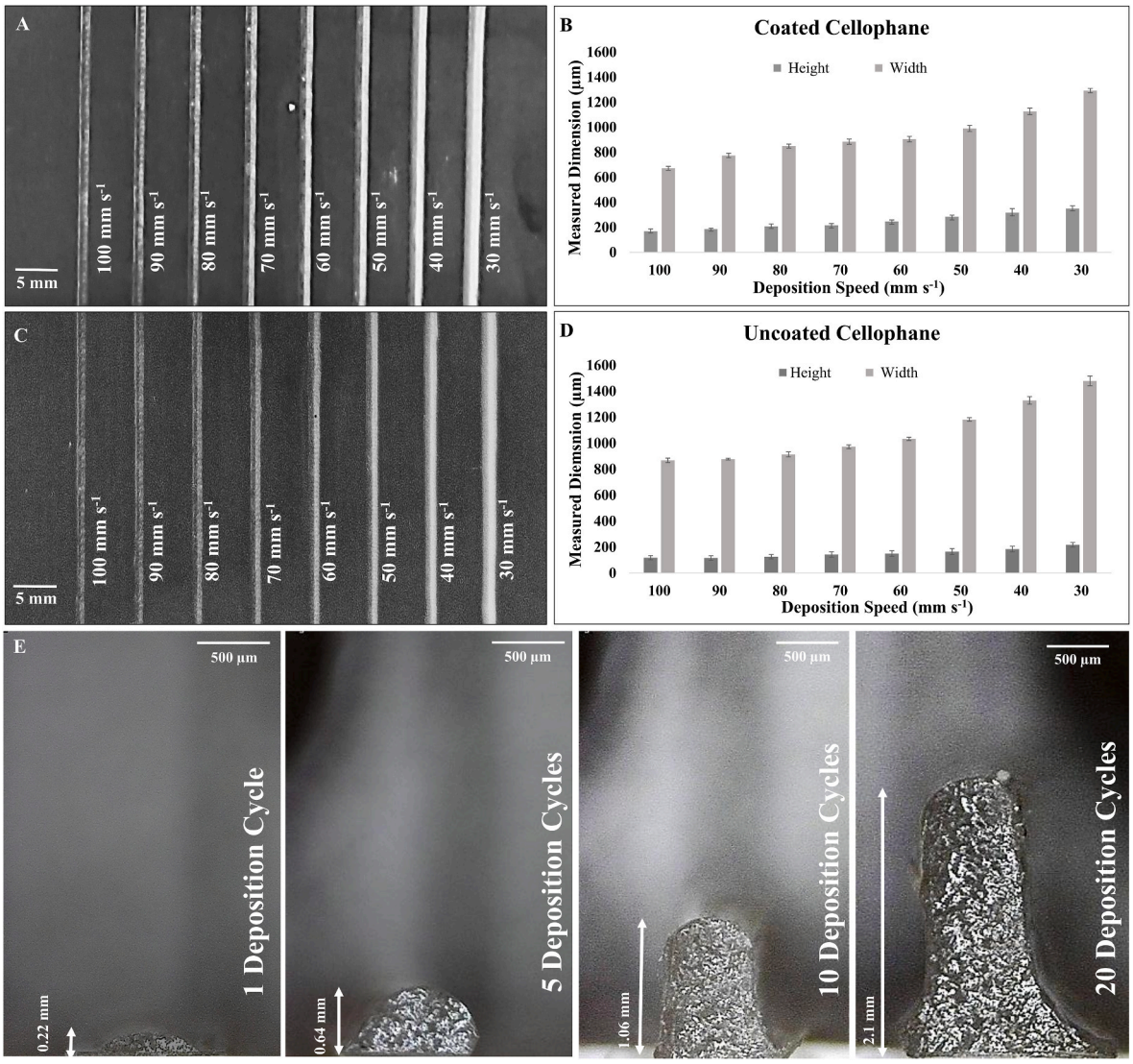

Fig. 2. LDW-patterned photo-polymer structures on cellophane using different deposition speeds and photo-polymer deposition cycles. (A) Representative (scanner) images of photo-polymer lines patterned on coated cellophane at deposition speeds of 30–100 mm s^{-1} (single deposition cycle; identical curing conditions). (B) Corresponding profilometry measurements of height and width versus deposition speed on coated cellophane. Data represent mean ± SD for triplicate devices fabricated on independent days (n = 3). (C) Representative (scanner) images of photo-polymer lines patterned on uncoated cellophane at deposition speeds of 30–100 mm s^{-1}. (D) Corresponding profilometry measurements of height and width versus deposition speed on uncoated cellophane. Data represent mean ± SD for triplicate devices fabricated on independent days (n = 3). (E) Cross-sectional microscope images of walls fabricated on coated cellophane using increasing numbers of deposition–curing cycles (1, 5, 10, and 20 cycles), showing incremental height increase (scale bars as shown).

obtain cross-sectional profile of the flow channel (Fig. 3E) and further inform of the integrity of the polymer-cellophane interface.

2.4. Fluidic performance evaluation of open wells and enclosed flow channels

The integrity of the laser-patterned structures was evaluated by testing their ability to confine fluids without any leakage or structural failure such as delamination from the substrate. For openwell microplate devices, each well was initially filled with 50 µL of a coloured dye (Brilliant Blue or Allura Red or Yellow) and then visually inspected every 5 min over a 30 min period for any evidence of leakage or structural deformation using a smartphone camera (Infinix Hot 50).

Enclosed flow channels were evaluated for both passive capillary driven (pump-free) and pump-driven flow. Passive capillary flow was characterised for hybrid channels fabricated with an uncoated cellophane (as the bottom layer) sealed with a coated cellophane (top layer). Flow channels with a nominal width of 1 mm were tested by pipetting 20 µL of an aqueous solution of coloured dye (Brilliant Blue FCF) into the inlet reservoir. The progression of the fluid front along the channel was recorded using a smartphone camera. The recorded videos were analysed to qualitatively confirm pump-free wicking and identify any potential leakage.

Pump-driven flow experiments were performed for the devices that had coated cellophane sheets as their top and bottom layers. A programmable syringe pump (New era pump systems, Inc. Model NE-4000) was used to introduce an aqueous solution of Allura Red dye from the inlet port of the enclosed flow channels. The structural integrity of the laser-patterned walls and therefore the flow channels was tested at five distinct flow rates of 50, 100, 150, 200, and 250 µL min^{-1}, with devices visually monitored throughout the experiment for signs of leakage due to any discontinuity of the wall structure or its delamination from the cellophane.

Burst-pressure testing was also performed for enclosed flow channel devices connected by an external tubing to a pressure sensor and a syringe. The inlet pressure was increased until visible leakage or structural

failure was observed. The burst pressure was recorded as the pressure at which leakage, delamination, or loss of sealing first became visible. The burst-pressure testing setup is shown in Fig. S1.

To further examine the flow behaviour within the enclosed flow channels and assess their suitability for passive mixing, devices incorporating a T-junction and a serpentine geometry were tested. Brilliant Blue FCF and Allura Red dye solutions were simultaneously introduced via the two inlets at a constant flow rate of 100 μL min^{-1} each into the channels with a 500 μm width and the resulting flow and the diffusion interface were observed and imaged with a smartphone camera.

2.5. Colourimetric detection of glucose and nitrite

Both types of devices, open wells and enclosed flow channels were next tested to explore their usefulness for colourimetric detection of nitrite and glucose.

2.5.1. Open wells

Nitrite (Griess reaction): Griess reagent was prepared immediately before use by mixing equal volumes of 1 % (w/v) sulfanilamide in 5 % (v/v) phosphoric acid and 0.1 % (w/v) N-(1-naphthyl) ethylenediamine dihydrochloride (NED).

Glucose (GOx/HRP–o-dianisidine): The glucose reagent was prepared by dissolving glucose oxidase/peroxidase (GOx/HRP) to a final activity of 10 U mL^{-1} and o-dianisidine dihydrochloride to 0.5 mg mL^{-1} in 0.1 M phosphate buffer (pH 6.0).

LDW-patterned open wells (7.5 mm diameter; 0.5 mm height achieved by 5 deposition-polymerisation cycles) were fabricated on uncoated cellophane. To start, 10 μL of the reagent (Griess or GOx/HRP–o-dianisidine) was dispensed into each well and dried at 37 °C for 2 h in an incubator. To evaluate the short-term stability of the assay reagents, dried and stored within the device, selected open well devices were stored at room temperature for one week before use. Calibration standards were prepared in 1 × PBS (glucose: 0–100 μg mL^{-1}; nitrite: 0–200 μM). For each measurement, 20 μL of the standard sample was added to the corresponding well and incubated for 15 min at room temperature. For further evaluation, artificial urine prepared as previously described (Brooks and Keevil, 1997) was spiked with glucose or nitrite at selected concentrations was used to test the open wells. The composition of artificial urine is provided in Table S1.

After incubation, images of the devices were acquired under fixed acquisition settings using an Epson V800 flatbed scanner (600 dpi) and saved in a RGB TIFF format. Images were analysed in ImageJ using a circular region of interest (ROI) of a fixed diameter, centered over each well while avoiding the well boundary. The mean grey values (MGV) were extracted from the RGB channel providing a maximum contrast for the assay product (magenta for the Griess assay product and brown for the glucose assay product). Signals were calculated as $\Delta MGV = MGV_{blank} - MGV_{sample}$. Calibration curves were generated by linear regression of ΔMGV versus analyte concentration. The limit-of-detection and limit-of-quantification were calculated as $LOD = 3\sigma_{blank}/slope$ and $LOQ = 10\sigma_{blank}/slope$, where σ_{blank} is the standard deviation of the signal acquired for a blank well which was incubated with just 1x PBS.

For artificial urine samples, concentrations were back-calculated from the PBS calibration using $C_{measured} = (\Delta MGV - intercept)/slope$, and recovery was reported as $\%Recovery = (C_{measured}/C_{spiked}) \times 100$. All measurements were performed in triplicate wells across three independent days (n = 9). The raw calibration datasets and artificial urine recovery calculations are provided in Table S2–S5.

2.5.2. Hybrid enclosed flow channels

Hybrid enclosed flow channels were fabricated using an uncoated cellophane bottom layer sealed with a coated cellophane top layer (Fig. 1C), following the fabrication procedure described in Section 2.2.3. Colourimetric reagents were pre-stored on the uncoated bottom layer at a designated detection zone prior to sealing.

For nitrite detection, Griess reagent was prepared immediately before use and 5 μL of the reagent was dispensed on the detection zone on the uncoated bottom layer and dried at 37 °C for 2 h. Devices were then sealed to form enclosed flow channels. Buffered nitrite or artificial urine standards were introduced into the inlet reservoir (typical volume 10 μL, sufficient to fill the channel and detection zone) and incubated for 15 min at room temperature (25 °C) to allow colour development.

For glucose detection, the GOx/HRP–o-dianisidine reagent was prepared and 5 μL of the reagent was dispensed on the detection zone on the uncoated bottom layer and dried at 37 °C for 2 h prior to sealing. Buffered glucose or artificial urine standards were introduced into the inlet (typical volume 10 μL) and incubated for 15 min at room temperature (25 °C).

After incubation with the standard samples, devices were imaged using an Epson V800 flatbed scanner (600 dpi) under fixed acquisition settings and saved in a RGB TIFF format. Enclosed flow channel measurements were performed as single-device demonstrations (n = 1 per concentration) and are presented as proof-of-concept for assay operation within enclosed flow channels.

3. Results and discussion

3.1. Fabrication control and device optimisation

A systematic study was conducted to establish a robust and reproducible control over the geometry of polymeric structures patterned on the surfaces of cellophane. The influence of key LDW parameters, namely the (photo-polymer) deposition speed and the number of deposition cycles on the final dimensions of a LDW patterned polymeric wall (shaped as a straight line) was investigated.

The deposition speed was identified as a critical parameter directly influencing both the width and height of the polymerised wall. As shown in Fig. 2A-2D, for a single deposition cycle, an inverse relationship was observed between deposition speed and feature dimensions. All values reported here represent mean ± SD values calculated for triplicate devices fabricated on three independent days, supporting the reproducibility of the fabrication process. At the slowest speed of 30 mm s^{-1}, wider and higher walls were produced with widths of ~1.3 mm, and heights ~350 μm on coated cellophane and widths ~1.5 mm and heights ~220 μm on uncoated cellophane. In contrast, the highest speed of 100 mm s^{-1} resulted in significantly narrower features with widths ~0.7 mm and heights of ~170 μm on coated cellophane and width of ~0.8 mm and heights of ~120 μm on uncoated cellophane.

This behaviour can be attributed to the fluid dynamics of the polymer jetting process. At higher traverse speeds, the photo-polymer volume deposited per unit length is relatively reduced. Representative profilometry measurements of mean values calculated from three measurements across triplicate devices qualitatively confirm this trend for both coated (Fig. 2B) and uncoated cellophane (Fig. 2D). These results demonstrate that deposition speed is an effective parameter for tuning the spatial resolution i.e., the wall height and wall width of the LDW patterned fluidic architectures.

To create walls with a higher aspect ratio, the influence of multiple deposition cycles as a parameter for providing additional control over the height (z-dimension) of LDW patterned flow channels was investigated at a fixed deposition speed for 50 mm s^{-1} identified from the preceding experiments. The relationship between the number of deposition cycles (1-20) and the resulting wall height was found to be quasi-linear, as depicted in Fig. 2E.

At a deposition speed of 50 mm s^{-1}, increasing the number of cycles resulted in a highly predictable, incremental increase in wall height, from approximately 220 μm for a single cycle to over 2.1 mm for 20 deposition cycles on coated cellophane. This linear correlation is advantageous, as it provides a straightforward and reliable method for engineering channels of a desired height. Precise control over the wall

height is crucial for applications requiring defined channel volumes, managing fluidic resistance in complex networks, and for fabricating structures necessary to realise devices with enclosed flow channel geometries, as discussed later.

Based on this systematic study, a set of fabrication parameters that enable the consistent creation of high-fidelity LDW patterned open wells and enclosed flow channels was established. These parameters comprise a photo-polymer deposition speed of 50 mm s^{-1} and laser curing speed of 30 mm s^{-1}. Under these conditions hydrophobic structures with widths ranging from ~1.2 mm to ~2 mm and heights ranging from ~0.17 mm to ~2 mm can be reproducibly fabricated.

3.2. Device morphology and interfacial properties

Based on the parameters defined above, open wells (Fig. 3A), straight channels (Fig. 3B), serpentine channels (Fig. 3C) and T-shaped channels (Fig. 3D) were fabricated on coated cellophane. Images of these structures were taken by using an Epson V800 flatbed scanner (600 dpi) and these demonstrate that LDW yields structures with smooth surfaces, indicative of uniform and complete laser-induced polymerisation.

The physical morphology of the fabricated structure and the quality of their interface with the cellophane substrate are critical determinants of device performance. Optical microscopy was thus used to further investigate the integrity of the polymer walls produced by the LDW process. As shown in Fig. 3E, cross-sectional microscopy image of the flow device reveals a seamless and robust polymer-cellophane interface, with strong adhesion of the polymer to the underlying coated cellophane substrate. No evidence of gaps, cracks, or delamination was observed, which is essential for the formation of leak-proof channels capable of withstanding fluid pressure during operation.

Although the interfacial chemistry was not fully understood, adhesion of the polymer to cellophane can be plausibly explained by the hydroxyl-rich, highly wettable nature of uncoated (hydrophilic) cellophane (Yamane et al., 2006), the reduced permeability of coated cellophane and mechanical anchoring (Packham, 2011). In addition to mechanical anchoring, the hydroxyl-rich, regenerated cellulose surface of uncoated cellophane with comparatively better wetting properties would promote polar interactions with the polymer and contribute to the adhesion. Coated cellophane is hydrophobic in nature, has a reduced permeability, and adhesion is therefore expected to be predominantly mechanical.

3.3. Fluidic performance evaluation of open wells and enclosed flow channels

3.3.1. Fluid holding capability of open wells

The capability of LDW patterned open wells to contain liquids was evaluated by dispensing 50 μL of a coloured dye solution into each well and monitoring the devices for 30 min for visible leakage or structural deformation (Fig. 4A and B). Wells ($n = 5$) patterned on both coated and uncoated cellophane maintained complete liquid confinement throughout the observation period, with no visible leakages, indicating effective containment and robust continuity of the walls.

Wells fabricated on coated cellophane showed no observable dimensional changes during liquid exposure (Fig. 4A). In contrast, wells patterned on uncoated cellophane exhibited substrate swelling (Fig. 4B), consistent with hydrophilic and water permeable nature of uncoated cellophane, reported previously (Hamedi et al., 2016). Importantly, this swelling did not compromise the structural integrity of the wells; they remained intact and no evidence was observed of cross-contamination between adjacent wells over the test duration.

3.3.2. Pump-driven flow in enclosed flow channel devices formed on coated cellophane

The robustness of the LDW-patterned enclosed flow channel devices was evaluated under pump-driven flow using devices assembled with coated cellophane as both the bottom and top layer. Because the coated cellophane films are hydrophobic, they do not support capillary driven flow; therefore, liquid transport in these devices requires external pumps.

Structural robustness of these sealed channels was first assessed in a straight channel device (Fig. 4C) by pumping an aqueous red dye solution at flow rates of 50-250 μL min^{-1}. Across all tested flow rates, no visible leakage, barrier failure, channel deformation, or delamination was observed, confirming LDW-patterned photo-polymer barriers and sealing approach withstand pump-driven operation over this range. Across the devices, burst-pressure tests showed apparent failure for pressures ranging from 143 to 352 mbar. The failure does not happen along the channel but instead was always observed at the polymer-glue interface at the outlet port. The results suggest that the measured values represent the burst pressure of the assembled device and not the intrinsic burst pressure of the laser-patterned flow channel. Importantly, the devices operated without leakage during pump-driven flow at 50–250 μL min^{-1}, indicating their operation was well below measured burst-pressures.

Following integrity testing, flow behaviour was examined in a T-junction device (Fig. 4E) by introducing two differently coloured dye solutions through separate inlets at a constant flow rate. Stable co-flow with a well-defined interface was observed at the junction and along the downstream channel, consistent with laminar transport. To further visualise downstream mixing behaviour under pump-driven conditions, a serpentine channel architecture (Fig. 4F) was used to carry two dye streams (yellow and blue), where the interface progressively broadened along the channel path, indicating diffusion-driven mixing during transport.

3.3.3. Pump-free passive flow in hybrid enclosed flowchannel devices formed on uncoated and coated cellophane

Passive, pump-free transport was achieved using a hybrid enclosed flowchannel device geometry fabricated with an uncoated (hydrophilic) cellophane bottom layer sealed by a polymer-coated (hydrophobic) cellophane as the top layer (Fig. 4D and 4G). A fully uncoated/uncoated format was not used because the top uncoated film exhibited poor sealing robustness, with a tendency for peeling/delamination during assembly and wet operation. In addition, placing the uncoated film as the bottom layer provides a hydrophilic surface suitable for reagent adsorption needed to support the subsequent implementation of dried assay chemistries in the channel.

In the hybrid configuration, the combination of a hydrophilic uncoated bottom surface and hydrophobic top surface generates a wettability contrast within the confined geometry, enabling capillary driven transport and spontaneous filling without external pumping as reported previously (Shigemori et al., 2023). Upon introducing an aqueous blue colour dye solution into the partially open inlet reservoir, the liquid front advanced along the straight channel by capillary action (Fig. 4D). Time-stamped images (Fig. 4D) were used to estimate the position of liquid flow-front during passive filling. The liquid front advanced by 41.0 mm within 25 s confirming rapid pump-free filling of the channel. To assess if the flow behaviour was of the Washburn-type, L^2 was plotted against time, yielding a value of $L^2 = 72.68t - 310.19$ with a $R^2 = 0.942$, supporting capillary-driven transport in the hybrid channel. These results demonstrate reliable passive, pump-free actuation in the hybrid format, supporting simplified operation for portable standalone assay workflows.

The same hybrid concept was also implemented in a T-junction geometry (Fig. 4G). When two dyed solutions were introduced by pipetting through separate inlets, stable co-flow was observed downstream from the junction, producing a distinct interface characteristic of laminar flow in confined channels. Collectively, these results demonstrate that hybrid enclosed flowchannel devices can support both pump-free fluid transport in simple channel layouts and controlled multi-inlet flow in more complex geometries.

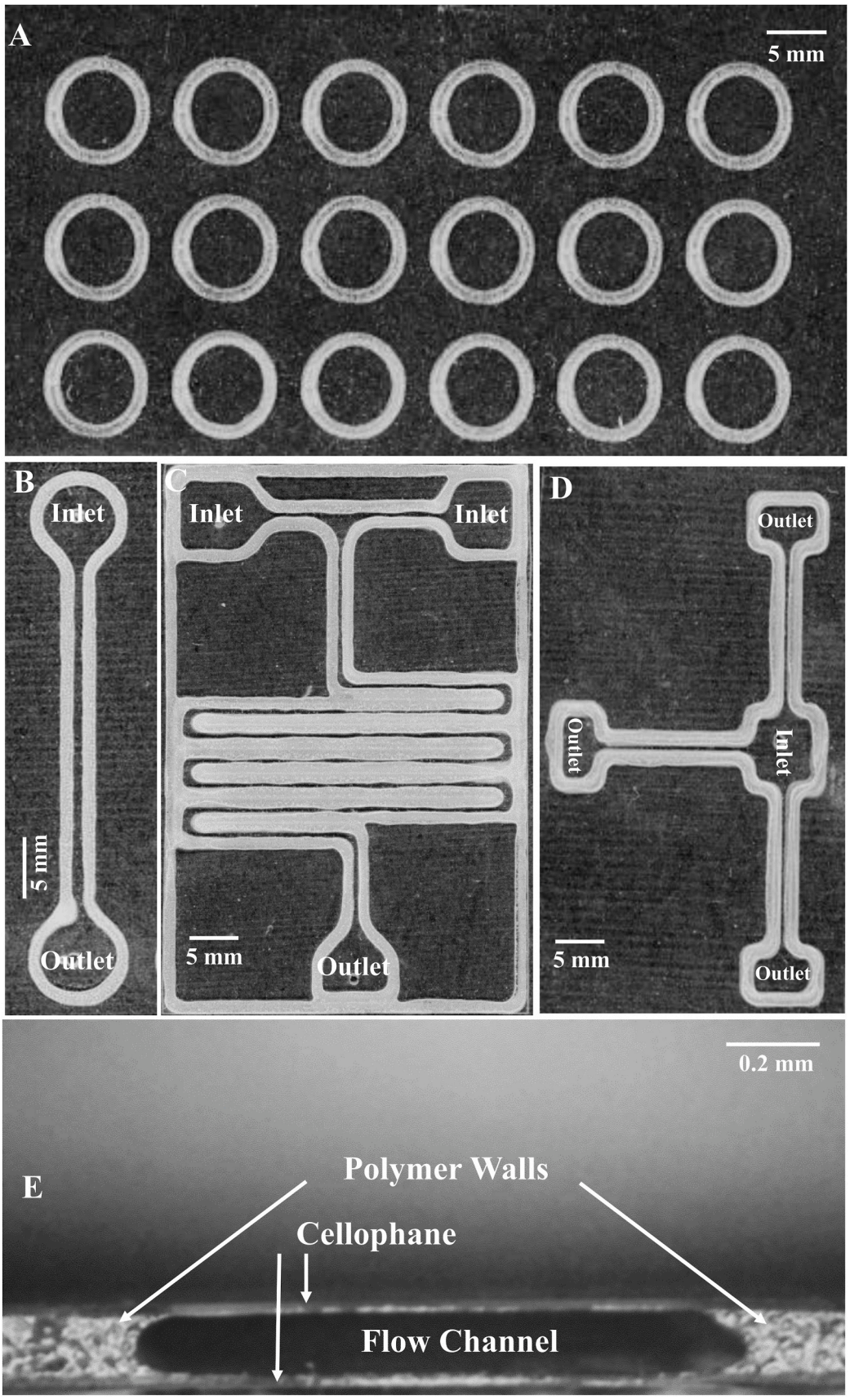

(caption on next page)

Fig. 3. Representative LDW-patterned cellophane device architectures and enclosed flow channel cross-section. (A) Top-down image of a LDW-patterned open well microplate array on coated cellophane. (B) Straight enclosed channel fluidic device with circular inlet and outlet reservoirs on coated cellophane. (C) Enclosed flow channel device with a serpentine channel geometry on coated cellophane. (D) Enclosed flow channel device with a T-junction geometry on coated cellophane. Panels (B–D) illustrate the continuity and definition of the laser-cured photo-polymer walls that form the channel boundaries (scale bars as indicated). (E) Cross-sectional micrograph of a representative enclosed flow channel device, showing the coated cellophane layers, cured photo-polymer walls, and the sealed channel lumen.

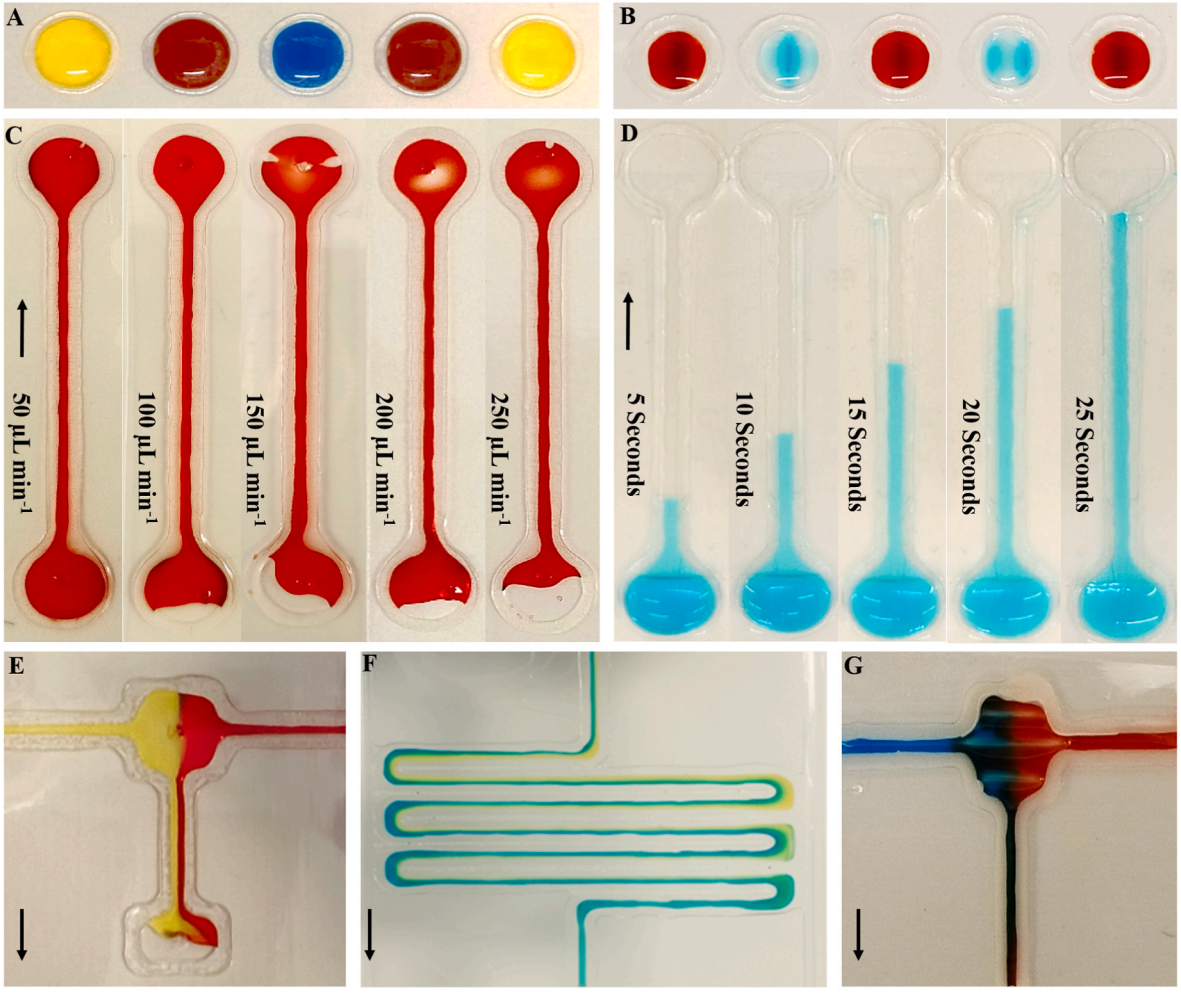

Fig. 4. Fluidic performance of LDW-patterned wells and closed channels on cellophane. (A, B) Open well arrays patterned on (A) coated and (B) uncoated cellophane, demonstrating containment of coloured dyes. (C) Pump-driven flow in enclosed flow channel device (coated top and bottom layers) at flow rates of 50–250 µL min^{-1}, showing stable transport without visible leakage. (D) Time-lapse images of passive, capillary-driven transport in a hybrid enclosed flow channel device (uncoated bottom layer sealed with a coated top layer), showing progression of the dye front at 5–25 s; the liquid front advanced approximately 41.0 mm within 25 s. (E) Enclosed flow channel T-junction devices formed using coated cellophane (top and bottom) demonstrating laminar co-flow of coloured dye solutions. (F) Enclosed serpentine channel formed using coated cellophane (top and bottom) showing diffusion-driven mixing (further along the channel). (G) Hybrid closed-channel T-junction devices formed on coated (top) and uncoated (bottom) cellophane demonstrating laminar co-flow of coloured dye solutions.

3.4. Colourimetric detection of nitrite and glucose

3.4.1. Assay within open wells

Devices laser patterned on uncoated cellophane to have an array of circular wells with a geometry comparable to commonly used microwell plates were evaluated as the primary platforms for the quantitative detection of nitrite and glucose.

Glucose detection: A concentration-dependent colour development was observed following addition of glucose to wells containing pre-dried GOx/HRP–o-dianisidine reagent (Fig. 5A). To minimise variability from ambient lighting and imaging conditions, all images were acquired using an Epson V800 flatbed scanner at 600 dpi under fixed acquisition conditions. Quantification by image analysis produced a linear calibration over the range of 10–100 µg mL^{-1} (Fig. 5C). The glucose calibration curve in buffer was generated by plotting the mean ΔMGV (blank-subtracted grayscale intensity) against glucose concentration (10–100 µg mL^{-1}). Each concentration was measured in triplicate on three independent days (n = 9 per concentration) resulting in a linear relationship (y = 0.3816x - 0.254: R^2 = 0.9888 for n = 9) between ΔMGV and glucose concentration. Using the blank standard deviation (σ_{blank} = 0.93) and the calibration slope, the LOD and LOQ were calculated as 7.31 µg mL^{-1} and 23.8 µg mL^{-1}, respectively.

Glucose-spiked artificial urine samples tested in the open wells showed close agreement with the PBS calibration at mid to high concentrations. Calculated concentrations were 42.5, 54.1, 73.2, and 97.0 µg mL^{-1} for nominal spikes of 40, 55, 75, and 100 µg mL^{-1}, corresponding to recoveries of 106.4 %, 98.3 %, 97.7 %, and 97.0 %, respectively.

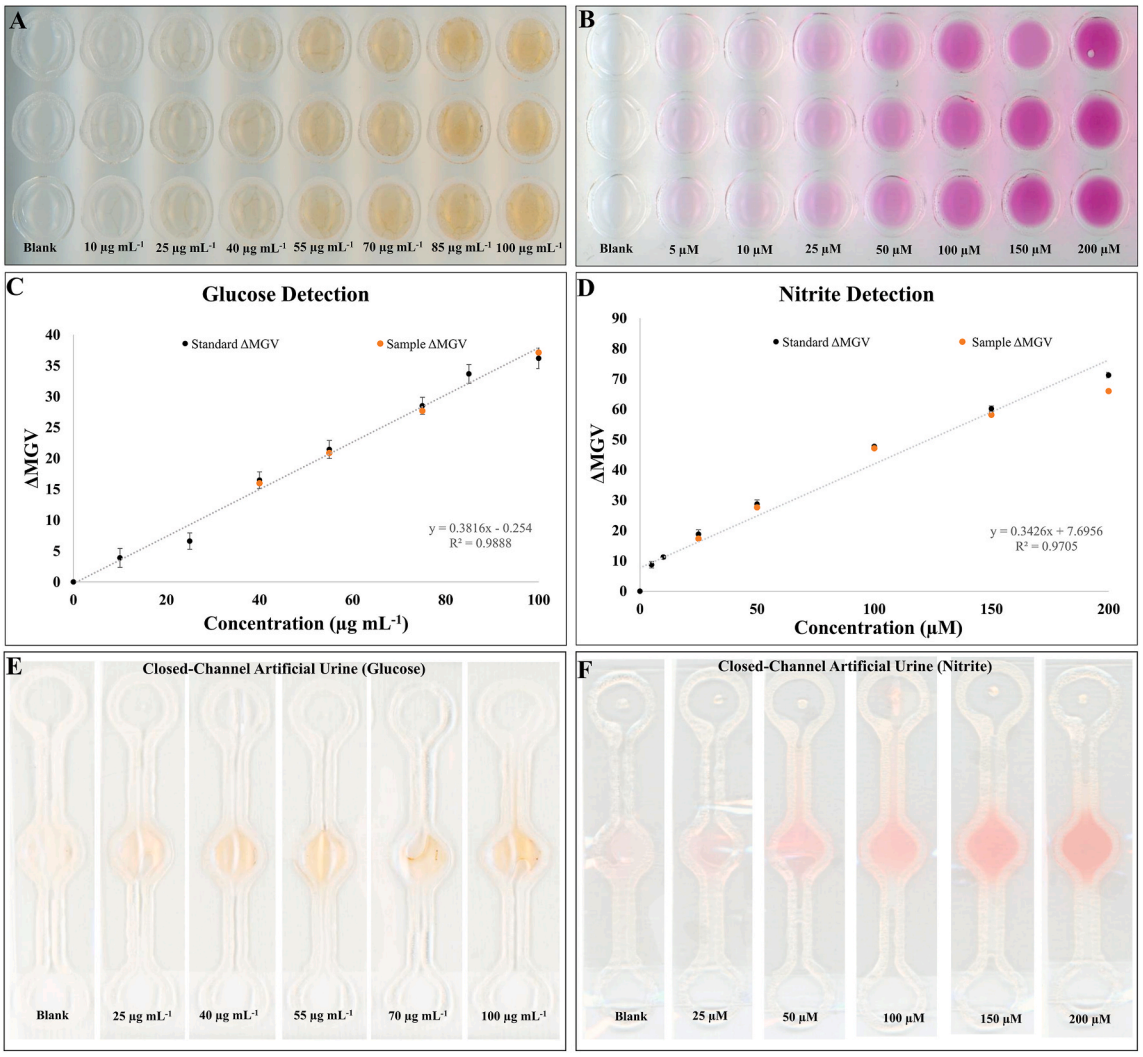

Fig. 5. Colourimetric detection of glucose and nitrite in LDW-patterned cellophane devices. (A) Open-well microplate assay for glucose showing concentration-dependent colour development for PBS standards (0–100 µg mL^{-1}). (B) Open-well microplate assay for nitrite (Griess reaction) showing concentration-dependent colour development for PBS standards (5–200 µM). (C) Glucose calibration in open wells obtained by plotting ΔMGV versus glucose concentration (black markers: PBS standards; orange markers: artificial urine spikes measured in open wells). (D) Nitrite calibration in open wells obtained by plotting ΔMGV versus nitrite concentration (black markers: PBS standards; orange markers: artificial urine spikes measured in open wells). Dashed lines indicate linear regression fits to the PBS standards (equations shown). For all quantification, images were analysed in ImageJ and ΔMGV was defined as ($MGV_{blank} - MGV_{sample}$). Error bars represent standard deviation (n = 9, triplicate measurements over three independent days). (E) Enclosed flow channel glucose assay performed using artificial urine spiked at concentrations selected to be above the open-well LOQ. (F) Enclosed flow channel nitrite assay performed using artificial urine spiked at concentrations selected to be above the open-well LOQ.

Nitrite detection: Nitrite was similarly quantified via the Griess reaction, producing a clear dose-dependent magenta colour in wells containing pre-dried Griess reagent (Fig. 5B). A linear calibration ($y = 0.3426x + 7.695692$; $R^2 = 0.971$ for n = 9) was obtained over a concentration range of 5–200 µM (Fig. 5D). Using the blank standard deviation ($\sigma_{blank} = 0.71$) and the calibration slope, the LOD and LOQ were calculated as 6.57 µM and 21.9 µM, respectively.

Nitrite-spiked artificial urine samples were evaluated over the range of 25–200 µM and concentrations were calculated using the PBS calibration curve. Recoveries of 115.8 % (25 µM), 117.4 % (50 µM), 114.9 % (100 µM), and 84.6 % (200 µM) were obtained, indicating a modest positive bias at low–mid concentrations and signal suppression at the highest concentration. Collectively, these results demonstrate that LDW-patterned open wells fabricated on uncoated cellophane support storage of dried colourimetric reagents to enable quantitative image-based readout in both buffer and artificial urine. The hydrophobic LDW structures provided robust fluid confinement and reproducible reaction volumes, thereby preventing cross-contamination between adjacent wells.

To evaluate the short-term stability of the dried and stored assay reagents, devices were stored at room temperature for one week before testing. These devices remained functional and produced visible colourimetric change on the addition of samples, supporting preliminary evidence of the compatibility of using dried and stored reagents within the LDW fabricated cellophane devices.

To contextualise the analytical performance of the LDW fabricated cellophane devices, their LODs were compared with representative colourimetric glucose and nitrite sensors reported in the literature (Table S6). Although substantially lower LODs have been reported for highly optimised electrochemical sensing platforms, the LDW-patterned cellophane devices show performances comparable to several colourimetric paper- and film-based devices. The glucose and nitrite assays were model colourimetric chemistries used to merely demonstrate reagent compatibility, testing with a urine-like matrix and image-based quantification of the fluidic devices, which are not fully optimised sensing systems intended for use as state-of-the-art analytical sensors.

3.4.2. Assays in hybrid enclosed flow channels

The colourimetric assays were further implemented in sealed, hybrid enclosed flowchannel devices to demonstrate the applicability of the LDW fabrication method (Fig. 5E and F). Hybrid enclosed flowchannel devices (comprising an uncoated bottom layer sealed with a coated top layer) were prepared with pre-dried Griess reagent (for nitrite detection) or GOx/HRP–o-dianisidine reagent (for glucose detection) patterned within a defined detection zone. Artificial urine samples spiked with nitrite or glucose were then introduced into the inlet reservoir to fill the channels and wet the detection region. In both cases, visible colour development was observed within the detection zones after incubation, confirming that the sealed, channel architecture supports enclosed liquid sample handling and that the cellophane–photo-polymer materials system is compatible with the colourimetric chemistries employed.

These enclosed flow channel experiments were performed as proof-of-concept demonstrations and were not quantified with the same statistical rigour as the open wells. Nevertheless, they validate the feasibility of reagent pre-storage and colourimetric reactions within sealed LDW-fabricated channels, providing a route towards more integrated cellophane-based fluidic workflows using the same fabrication approach.

Although individual interfering species usually present in urine were not tested separately to evaluate the specificity, artificial urine used to test the devices contained common urinary components such as urea, uric acid, creatinine, and inorganic salts. Blank artificial urine samples produced no visible colour change, suggesting that the interfering substances within the artificial urine matrix do not result in false-positives for the tested conditions. Spiked artificial urine samples showed glucose and nitrite recoveries of 97.0–106.4 % and 84.6–117.4 % respectively, indicating compatibility in the use of an artificial urine matrix. This is not a full interference study that evaluates the assay specificity but is a study done to assess the compatibility of the assay/device with a contrived urine matrix.

Clinical urine samples were not evaluated in this study because the primary objective was to demonstrate the utility of the LDW methodology for the fabrication of fluidic devices on cellophane and further show the compatibility of these devices with colourimetric assays, and not to undertake clinical validation. Future studies will focus on evaluating the devices using clinical and/or environmental samples.

3.5. Overall assessment of the LDW method

A key advantage of the LDW method for cellophane-based fluidics is the combination of rapid fabrication and low material cost, enabling both rapid prototyping and scalable production. Using optimised parameters, fabrication of a complete 96-well geometry required approximately 4.0 g of polymer for five deposition cycles, while a straight channel required less than 0.5 g of polymer. Fabrication times from deposition to the finished device were 12.5 min and 2 min respectively for the 96-well format and the straight, enclosed flow channel. Based on the costs of photo-polymer and cellophane substrate, the cost of a 96-well device was estimated to be less than $0.50, while that of an enclosed-flow channel device was less than $0.10. These estimates are materials-only calculations based on photopolymer consumption, cellophane substrate area, and assumed unit material costs, and do not include equipment, labour, assay reagents, wastage, packaging, or manufacturing overheads; detailed assumptions are provided in Table S7 and S8. Preliminary dry tape-peel testing showed that 8/10 coated closed-channel devices and 9/10 hybrid closed-channel devices remained structurally intact after tape removal, demonstrating the mechanical robustness of the LDW-patterned structures (Fig. S2). Compared with conventional microfabrication workflows such as soft lithography, the LDW approach also eliminates the need for fabrication of moulds and enables on-demand design iteration with minimal setup time. Although injection moulding remains advantageous for high-volume manufacturing due to low unit cost after tooling, the LDW platform offers a practical and flexible route for both rapid prototyping and mass fabrication of disposable devices, including point-of-care diagnostic formats.

4. Conclusion

In conclusion, we have developed and demonstrated a laser direct-write (LDW) fabrication method for the rapid and low-cost production of cellophane-based fluidic devices. This approach addresses the limitations of previously reported cellophane-based fluidics fabrication approaches by eliminating the need for multi-step assembly processes (such as moulds, double-sided tapes and lamination layers). By avoiding tape-based bonding and lamination-sheet assembly, the LDW workflow reduces reliance on additional non-biodegradable components, thereby supporting the development of more environmentally sustainable disposable device architectures. The LDW method enables direct, software-defined patterning of hydrophobic photo-polymer patterns with controllable feature geometries. The resulting devices supported both pump-driven operation in fully coated enclosed flow channels and pump-free capillary-driven transport in hybrid enclosed flow channels. Quantitative colourimetric detection of glucose and nitrite was validated in open wells, yielding LOD/LOQ values of 7.31/23.8 μg mL^{-1} for glucose and 6.57/21.9 μM for nitrite (buffer calibrations) respectively. These results demonstrate compatibility with image-based readout for colourimetric assays with pre-stored and dried reagents. LDW-patterned devices remained structurally intact and showed no visible leakage after two weeks of storage before testing. In addition, devices containing the dried and stored assay reagents remained functional after one week of storage at room temperature. However, the long-term stability of stored reagents and therefore long-term shelf-life of LDW fabricated cellophane devices remain to be established. These results position LDW-patterned cellophane as a practical platform for the rapid development of disposable, optically transparent fluidic devices. Future work will focus on extending this approach to multiplexed assays, evaluating performance in more complex sample matrices and integrating the platform with portable readout systems, including smartphone-based image analysis.

CRediT authorship contribution statement

Ahsan Ali: Conceptualization, Data curation, Formal analysis, Investigation, Methodology, Writing – original draft. **Panagiotis Galanis:** Investigation, Resources, Writing – review & editing. **Jonathan McQuillan:** Investigation, Resources, Writing – review & editing. **Kordo Saeed:** Supervision, Writing – review & editing. **Ahilanandan Dushianthan:** Supervision, Writing – review & editing. **Gopalan K. Sivaraman:** Writing – review & editing. **Collin L. Sones:** Conceptualization, Funding acquisition, Methodology, Project administration, Supervision, Writing – review & editing.

Declaration of competing interest

The authors declare that they have no known competing financial interests or personal relationships that could have appeared to influence the work reported in this paper.

Acknowledgements

The authors also acknowledge the funding received from UK Research and Innovation - Engineering and Physical Sciences Research Council under “Grant No. UKRI823”. We thank Professor Xunli Zhang, Professor of Bioengineering at School of Engineering, University of Southampton for valuable comments and suggestions.

Appendix A. Supplementary data

Supplementary data to this article can be found online at https://doi.org/10.1016/j.biosx.2026.100809.

Data availability

Data will be made available on request.

References

Brooks, T., Keevil, C., 1997. A simple artificial urine for the growth of urinary pathogens. Lett. Appl. Microbiol. 24 (3), 203–206.

Budd, J., Miller, B.S., Weckman, N.E., Cherkaoui, D., Huang, D., Decruz, A.T., Fongwen, N., Han, G.-R., Broto, M., Estcourt, C.S., 2023. Lateral flow test engineering and lessons learned from COVID-19. Nat. Rev. Bioeng. 1 (1), 13–31.

Dincer, C., Bruch, R., Costa-Rama, E., Fernández-Abedul, M.T., Merkoçi, A., Manz, A., Urban, G.A., Güder, F., 2019. Disposable sensors in diagnostics, food, and environmental monitoring. Adv. Mater. 31 (30), 1806739.

Galanis, P., Katis, I., He, P., Iles, A., Kumar, A.J., Eason, R., Sones, C., 2022. Laser-patterned paper-based flow-through filters and lateral flow immunoassays to enable the detection of C-reactive protein. Talanta 238, 123056.

Gubala, V., Harris, L.F., Ricco, A.J., Tan, M.X., Williams, D.E., 2012. Point of care diagnostics: status and future. Anal. Chem. 84 (2), 487–515.

Hamedi, M.M., Ünal, B., Kerr, E., Glavan, A.C., Fernandez-Abedul, M.T., Whitesides, G. M., 2016. Coated and uncoated cellophane as materials for microplates and open-channel microfluidics devices. Lab Chip 16 (20), 3885–3897.

He, P., Katis, I., Eason, R., Sones, C., 2016. Laser direct-write for fabrication of three-dimensional paper-based devices. Lab Chip 16 (17), 3296–3303.

He, P.J.W., Katis, I.N., Eason, R.W., Sones, C.L., 2018. Rapid multiplexed detection on lateral-flow devices using a laser direct-write technique. Biosensors 8 (4), 97.

He, P.J.W., Katis, I.N., Kumar, A.J.U., Bryant, C.A., Keevil, C.W., Somani, B.K., Mahobia, N., Eason, R.W., Sones, C.L., 2020. Laser-patterned paper-based sensors for rapid point-of-care detection and antibiotic-resistance testing of bacterial infections. Biosens. Bioelectron. 152, 112008.

Hu, J., Wang, S., Wang, L., Li, F., Pingguan-Murphy, B., Lu, T.J., Xu, F., 2014. Advances in paper-based point-of-care diagnostics. Biosens. Bioelectron. 54, 585–597.

Katis, I.N., He, P.J.W., Eason, R.W., Sones, C.L., 2018. Improved sensitivity and limit-of-detection of lateral flow devices using spatial constrictions of the flow-path. Biosens. Bioelectron. 113, 95–100.

Makarov, I.S., Golova, L.K., Bondarenko, G.N., Anokhina, T.S., Dmitrieva, E.S., Levin, I. S., Makhatova, V.E., Galimova, N.Z., Shambilova, G.K., 2022. Structure, morphology, and permeability of cellulose films. Membranes 12 (3), 297.

Martinez, A.W., Phillips, S.T., Whitesides, G.M., Carrilho, E., 2010. Diagnostics for the developing world: Microfluidic paper-based analytical devices. Anal. Chem. 82 (1), 3–10.

Noviana, E., Ozer, T., Carrell, C.S., Link, J.S., McMahon, C., Jang, I., Henry, C.S., 2021. Microfluidic paper-based analytical devices: from design to applications. Chem. Rev. 121 (19), 11835–11885.

Ongaro, A.E., Ndlovu, Z., Sollier, E., Otieno, C., Ondoa, P., Street, A., Kersaudy-Kerhoas, M., 2022. Engineering a sustainable future for point-of-care diagnostics and single-use microfluidic devices. Lab Chip 22 (17), 3122–3137.

Packham, D.E., 2011. Theories of fundamental adhesion. In: da Silva, L.F.M., Öchsner, A., Adams, R.D. (Eds.), Handbook of Adhesion Technology. Springer Berlin Heidelberg, Berlin, Heidelberg, pp. 9–38.

Shigemori, H., Maejima, K., Shibata, H., Hiruta, Y., Citterio, D., 2023. Evaluation of cellophane as platform for colorimetric assays on microfluidic analytical devices. Microchim. Acta 190 (2), 48.

Solanki, S., Pandey, C.M., Gupta, R.K., Malhotra, B.D., 2020. Emerging trends in microfluidics based devices. Biotechnol. J. 15 (5), 1900279.

Sones, C., Katis, I., He, P., Mills, B., Namiq, M., Shardlow, P., Ibsen, M., Eason, R., 2014. Laser-induced photo-polymerisation for creation of paper-based fluidic devices. Lab Chip 14 (23), 4567–4574.

Tarim, E.A., Anil Inevi, M., Ozkan, I., Kecili, S., Bilgi, E., Baslar, M.S., Ozcivici, E., Oksel Karakus, C., Tekin, H.C., 2023. Microfluidic-based technologies for diagnosis, prevention, and treatment of COVID-19: recent advances and future directions. Biomed. Microdevices 25 (2), 10.

Whitesides, G.M., 2006. The origins and the future of microfluidics. Nature 442 (7101), 368–373.

Yager, P., Edwards, T., Fu, E., Helton, K., Nelson, K., Tam, M.R., Weigl, B.H., 2006. Microfluidic diagnostic technologies for global public health. Nature 442 (7101), 412–418.

Yamane, C., Aoyagi, T., Ago, M., Sato, K., Okajima, K., Takahashi, T., 2006. Two different surface properties of regenerated cellulose due to structural anisotropy. Polym. J. 38 (8), 819–826.

Yang, Q., Fukuzumi, H., Saito, T., Isogai, A., Zhang, L., 2011. Transparent cellulose films with high gas barrier properties fabricated from aqueous alkali/urea solutions. Biomacromolecules 12 (7), 2766–2771.

Zhang, L., Liu, H., Zheng, L., Zhang, J., Du, Y., Feng, H., 1996. Biodegradability of regenerated cellulose films in soil. Ind. Eng. Chem. Res. 35 (12), 4682–4685.

Zimmer, M., Laurenceau, E., Trombotto, S., Jamois, C., Deman, A.-L., 2026. Bio-based materials: an alternative to synthetic polymers for the development of lab-on-a-chip devices. Front. Lab Chip Technol. 4, 1703031.